SCIENTIFIC REPORTS
nature research

Check for updates

OPEN

Fabrication of multifunctional TANI/Cu_2O/Ag nanocomposite for environmental abatement

Sathish Mohan Botsa[1,2]✉ & Keloth Basavaiah[1]✉

During past decade, the ternary nanocomposite is ubiquitous in nanotechnology. Herein, a simple fabrication of cuprous oxide (Cu_2O) and silver (Ag) nanoparticles into Tetraaniline (TANI) matrix by in situ-polymerization approach to attain Tetramer-Metal Oxide-Metal (TANI/Cu_2O/Ag, shortly TCA) ternary composite was reported firstly. The synthesized materials were further characterized by a series of instrumental techniques to understand its structure, morphology and thermal properties. This nanocomposite showed promising applications in wastewater treatment by the testing of photocatalytic activity over the pararosaniline hydrochloride (PRA) dye degradation under visible light radiations, removal of Cadmium ion (Cd^{2+}) by adsorption, corrosion resistance and antibacterial activity against both gram positive and gram negative bacterial strains. The obtained results of TCA compared with the pure TANI and binary nanocomposite (TANI/Cu_2O) declared that the TCA composite is excellent material to solve the environmental issues due to lesser bandgap energy, visible light respond, high absorptivity, and long-life excitation.

Water has exploit asset on the earth, as concern for human beings, the water pollution is currently great issue throughout world and cause copious diseases almost leads to death[1,2]. In developing countries, the drinking water contamination by the second largest source mainly pesticides, chemical fertilizer residues and dyes are said to be concern agents[3]. The nanomaterials have enormous potential to deletion of heavy metals, organic pollutants, inorganic anions and bacteria have been reported[4–7]. Based on copious studies, the nanomaterials illustrate great importance for applications in purify the contaminated water.

As a result of the small size, large surface area, especially high mobility in solution, the nanomaterials ensure strong adsorption capacities and reactivity[8]. The nanomaterials exclusively metal oxide semiconductors have attracted by the scientists in evolving the pollute water treatment methods. Nanocatalysts (second class of nanomaterials) such as electrocatalysts, fenton based catalysts (photocatalysts) to developing for organic pollutants degradation and antimicrobial properties[9–11]. The number of processes has been employed yet but they are ineffective and moreover time consuming. For example, adsorption process converts the dyes from one form to another. Later the Advanced Oxidation Processes (AOP) embraces Fenton, photo Fenton, ozonisation, semiconductor based photocatalysis, photolysis have been developed for the effective decolouration of dye pollutants and destroy the microorganisms. In photocatalysis, the water and oxygen undergo redox reactions which produce extremely Reactive Oxygen Species (*OH, $*O_2-$) which are most accountable for the dyes degradation under light illumination[12]. Especially the semiconductor heterogeneous photocatalysis seems as better destructive technology to the total decolouration of dyes and destroy the microorganisms. Cuprous oxide (Cu_2O), a p-type semiconductor and has great attention in potential applications such as solar energy conversion, photocatalysis, sensors, CO oxidation and antibacterial agents due to cost-effective, splendid physicochemical properties, high absorption activity with narrow bandgap of 2.17 eV[13,14]. But the recombination rate of electron–hole pair is very fast due to its bandgap resulting in less photocatalytic degradation efficiency.

Recently, the scientific reports have been stated that the combination of conducting polymers with metal oxide serves as alternate materials for optoelectronic applications. Among the conducting polymers, Polyaniline (PANI) has gained a lot of attention past 20 years owing to its facile synthesis[4], chemical and environmental stability[5] and excellent electronic properties. Therefore, PANI was used widely as conducting polymer as easy and cost-effective synthesis, fast switching redox states, metallic behaviour, and versatile switching to its conductive state

[1]Department of Inorganic and Analytical Chemistry, Andhra University, Visakhapatnam 530003, India. [2]National Centre for Polar and Ocean Research, Ministry of Earth Sciences, Goa 403804, India. ✉email: bsathish401@gmail.com; klbasu@gmail.com

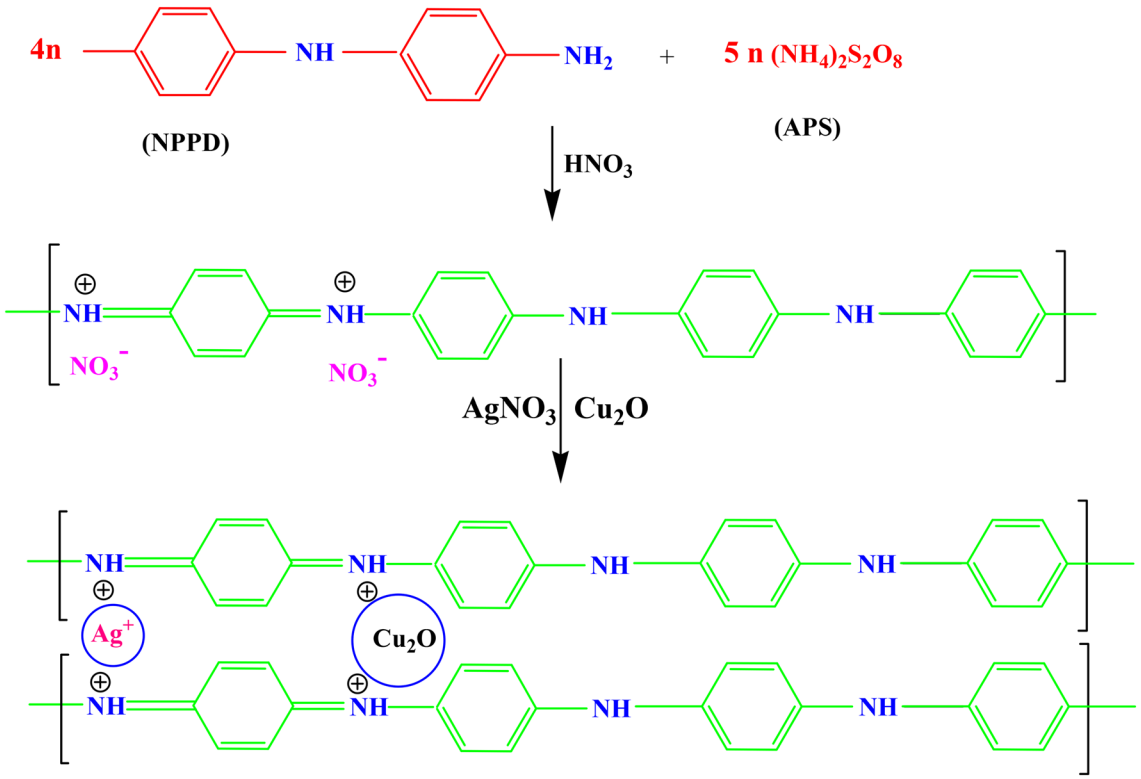

Figure 1. Formation mechanism of TANI/Cu_2O/Ag Nanocomposite.

through redox and protonic acid doping (with organic and inorganic acids)[15–17]. PANI has the vast applications in optical[18, 19] electronic[20, 21], biological fields[22,23] and as metal anti-corrosion[24] due to its superior conductivity and reversible re-oxidation. Tetraaniline (TANI) is aniline tetramer and has almost the same electrochemical properties as PANI[25]. However, due to its stiff structure, PANI is generally insoluble in aqueous solution, which limits its practical application[26,27]. Polymer and its nanocomposites possess unique characteristics when compared to other bulk materials due to improve the structure and controls their size range[28]. Semiconducting nature of PANI used to form nanocomposites with semiconductors (metal oxide) which are facilitating optical measurements. Though, the synthesis of monodispersed metal oxide nanoparticles into the polymer matrix of its nanocomposites with adaptable sizes and endangered from photooxidation is a major challenge. In meticulous, it is thorny to produce highly increased environmental concerns to resolve in such polymer and metal oxide nanocomposites systems. However, the silver (Ag) based composites with metal oxides gives better results in the photocatalytic efficacy by develop the charge transfer between dye molecules and metal oxides[17].

Hence, we attempted to appraise the synthesis and characterization of TANI/Cu_2O/Ag (TCA) ternary nanocomposite by a simple, eco-friendly and cost-effective *insitu* polymerisation method for solving the water concern issues such as pararosaniline dye degradation, removal of cadmium ions, corrosion inhibition and antibactericidal assay over the gram negative and positive bacteria.

Results and discussion

Formation mechanism of TANI/Cu_2O/Ag NC. Initially, the monomer NPPD undergoes protonation by react with HNO_3 to obtain the protonated ions in toluene medium and then the protonated ions undergo polymerization in presence of aqueous solution of APS. Here, the interjunction is formed between the toluene and aqueous media. The ions maces together and extend themselves into straight chain (1, 4 joining of phenyl groups) but the side products didn't occur due to the fast reaction of anilinium ions. The protonation occurs on imine unit of quninonoid part of EB (TANI) and removes lone pair of electrons on nitrogen so that gets positive charge. The free NO_3^- accumulates onto the EB (green colour) because of electrostatic attraction between NO_3^- and TANI. The copper ions (Cu^+) of Cu_2O and Ag^+ ions from $AgNO_3$ which accommodate onto TANI as presented in Fig. 1.

Characterisation study of prepared samples. *XRD study.* The pure phase formation of TANI, TANI/Cu_2O and TCA composite was confirmed by powder XRD and the diffraction peaks of prepared materials are presented in Fig. 2. The broad peak at $2\theta = 25°$ confirmed the presence of TANI[29] along with other two major peaks at 20.6° and 27.5° due to the periodicity of parallel and perpendicular to the phenyl ring of TANI which authorizes the (110) plane and the peak was presented at 14.6° declared that formed TANI is amorphous in nature, thus XRD peaks are not sharp. Further, TANI implies four peaks have been observed in TCA NC with 2θ values of 38.4°, 44.9°, 65°and 78° which are consistent to their respective planes (111), (200), (220) and (311). The presence of sharp peak at 39°confirmed that Ag NPs are embedded in TANI/Cu_2O/Ag matrix. The XRD

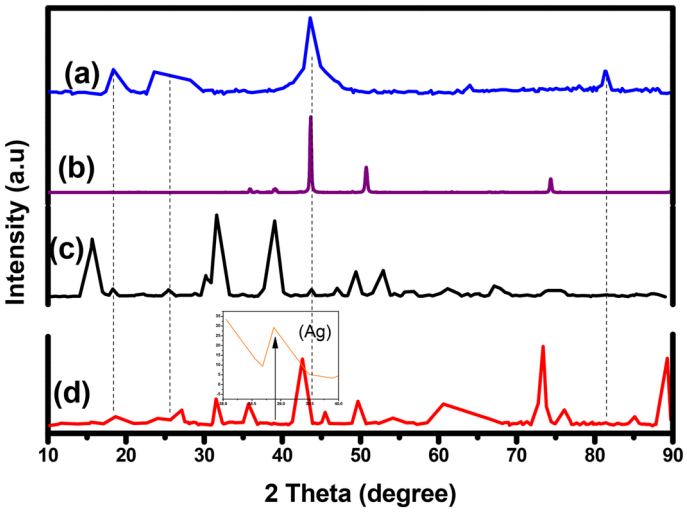

Figure 2. XRD patterns of (a) Cu_2O (b) TANI (c) TANI/Cu_2O and (d) TANI/Cu_2O/Ag.

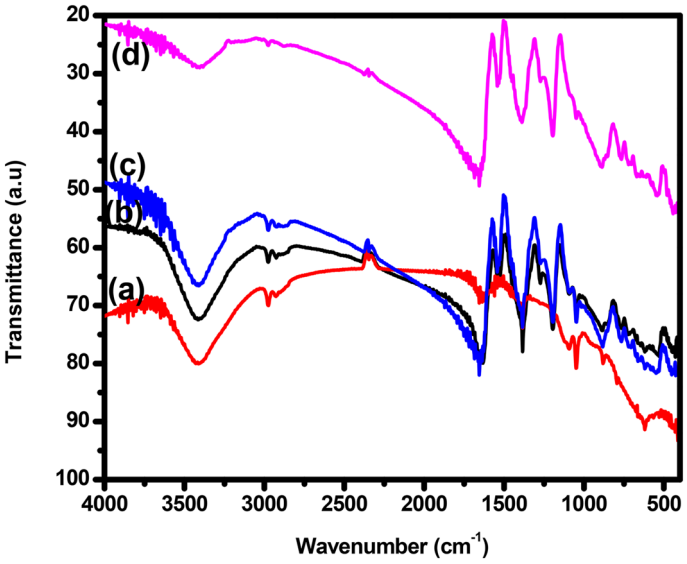

Figure 3. FTIR spectra of (a) Cu_2O (b) TANI (c) TANI/Cu_2O and (d) TANI/Cu_2O/Ag NCs.

pattern of Cu_2O NPs has sharp peak at $2\theta = 44°$ which corresponds to the (111) planes (standard JCPDS file No. 05-661) along with certain other peaks of low intensity[30]. However, these peaks show slightly shifted from their respective standard positions which may be due to the presence of Cu_2O and Ag into TANI matrix. These results are further compiled with FTIR.

FTIR analysis. The FTIR spectra of synthesized Cu_2O, TANI, TANI/Cu_2O and TCA NCs are depicted in Fig. 3. The broad absorption peak in the range of 750–550 cm^{-1} can be attributed to C–NO_3^- bonding is observed in TANI. The sharp peak appeared at 834 cm^{-1} due to N–H bending vibrations. Two peaks were observed at 1,163 cm^{-1} and 1,307 cm^{-1} could be assigned to the presence of quinonoid ring (N = Q = N) and C–N stretching mode vibrations respectively. The peaks were centred at 1581 cm^{-1} and 1,489 cm^{-1} are attributed to C–N and C–C stretching mode for quinonoid and benzenoid rings[31]. The intensities of these two peaks are almost confirms that the prepared TANI is conductive with emeraldine base (EB) form. Another peak was presented at 2,919 cm^{-1} is due to the C–H stretching vibrations whereas the peak at 3,382 cm^{-1} for the N–H stretching vibrations. These peaks were slightly shifted from their normal positions of pure TANI[32] owing to the existence of Cu_2O, Ag into TANI matrix.

FESEM–EDS analysis. The morphology and structural elemental composition of prepared Cu_2O, TANI, TANI/Cu_2O and TCA NCs were investigated by FESEM and EDS respectively. Figure 4a,b shows the FESEM

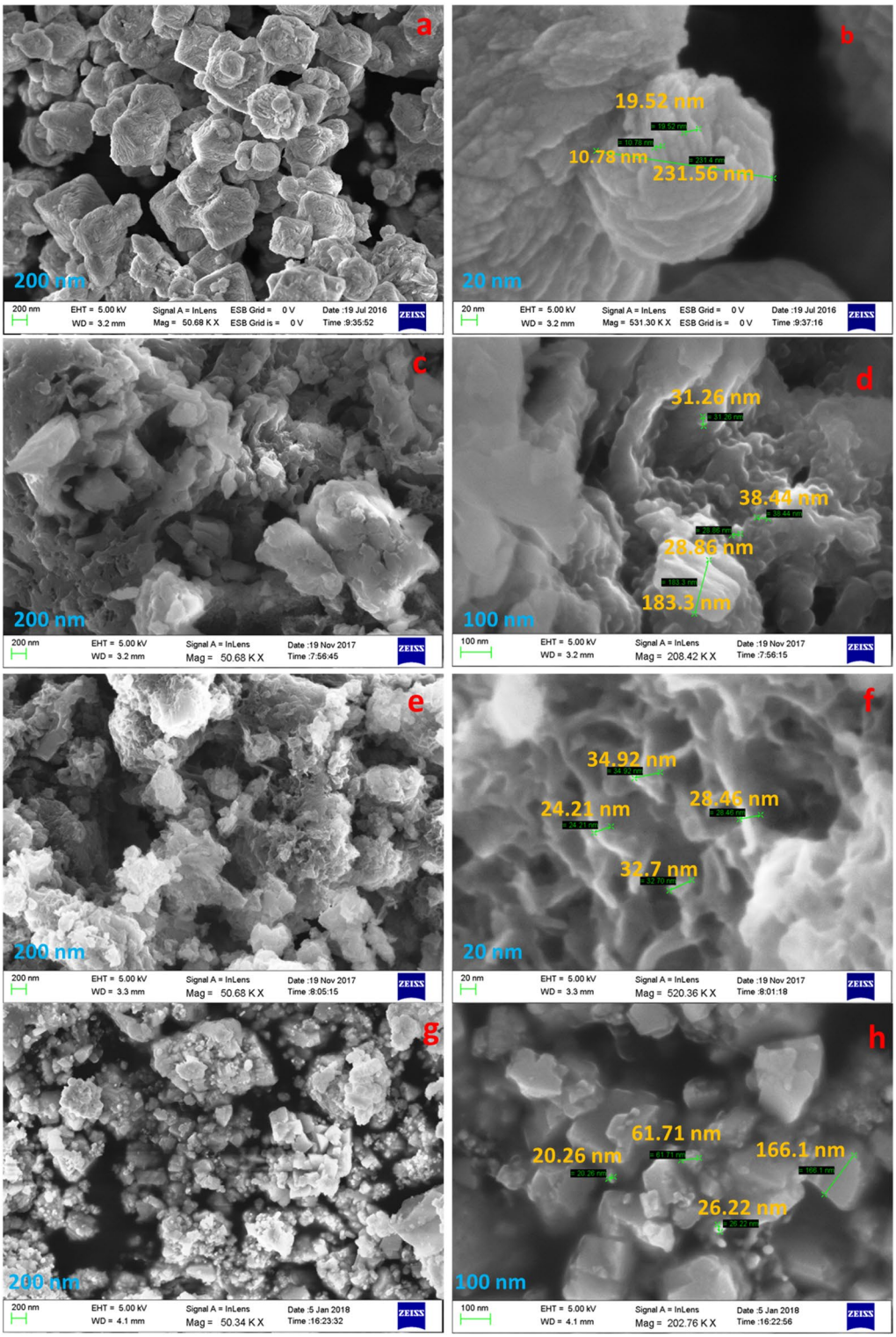

Figure 4. FESEM images of (**a**, **b**) Cu_2O, (**c**, **d**) TANI, (**e**, **f**) TANI/Cu_2O and (**g**, **h**) TANI/Cu_2O/Ag NCs.

images of Cu_2O clearly exhibited the octahedral like shape with smooth surface and an average edge length of about 478 nm. Figure 4c,d describes about the TANI, a clear and transparent sheet like structure was obtained. Figure 4e,f implies the FESEM images of TANI/Cu_2O, in which the Cu_2O are embedded in the matrix of TANI. It is clearly found that the surfaces of the prepared TCA NC were rough and uneven because of the presence of Ag and Cu_2O nanoparticles are decorated on the surface of TANI as shown in Fig. 4g,h.

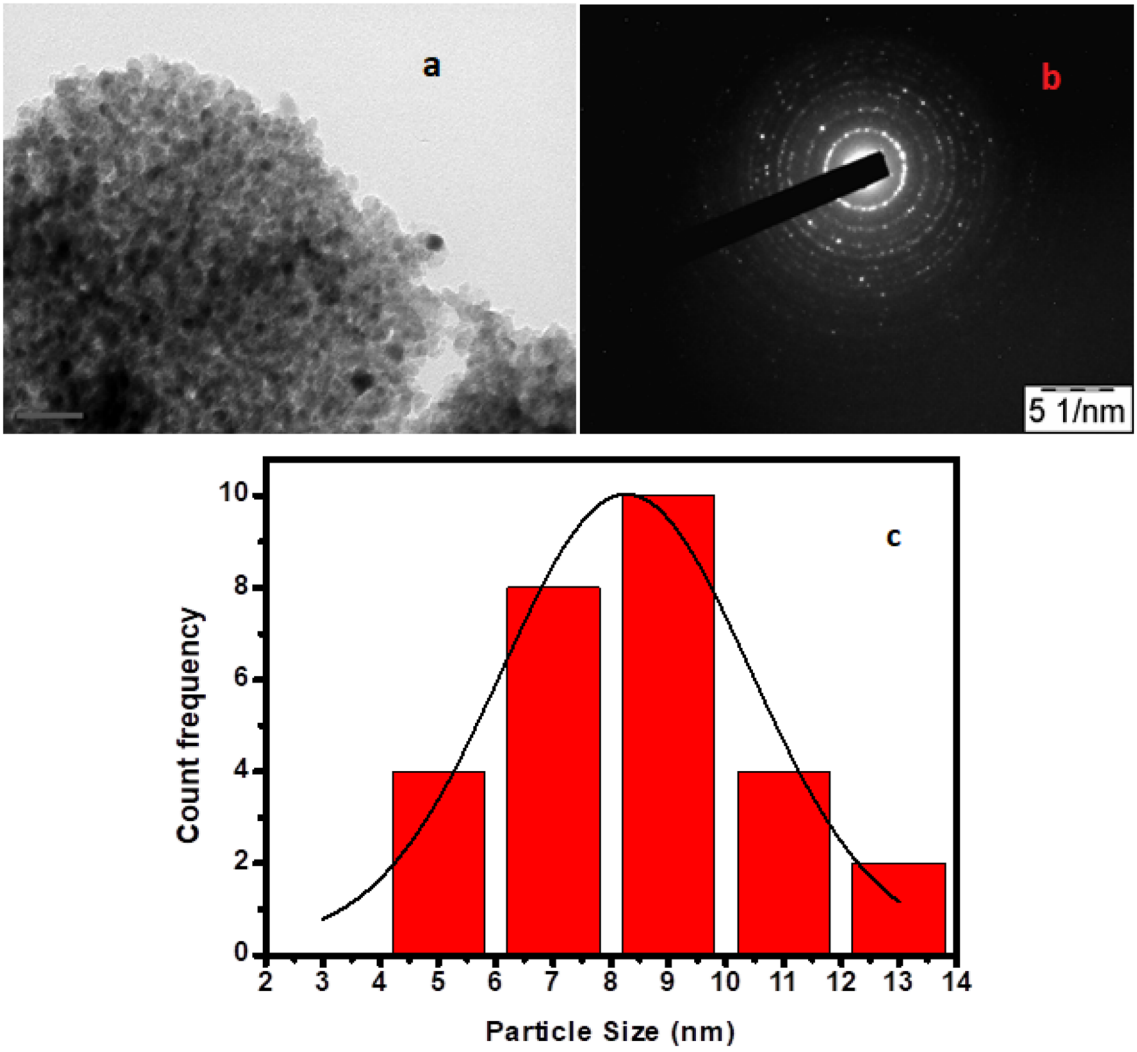

Figure 5. (**a**) TEM, (**b**) SAED image and (**c**) histogram of TANI/Cu_2O/Ag composite.

The presence of elements such as copper (Cu), oxygen (O), Silver (Ag), Carbon (C) and Nitrogen (N) in the EDS spectrum was confirmed the formation of pure TCA via a simple, facile *insitu* polymerization method (Fig S1).

Transmission emission microscopy (TEM). Further morphology of prepared TCA NC was studied using HRTEM and Selected area electron diffraction (SAED); the images (Fig. 5a,b) indicated a poor crystalline nature of NC, supported by XRD results. It is in well agreement with the diffraction planes of TCA NC. The average particle size of TCA NC was 8.26 nm calculated from histogram (Fig. 5c) using imageJ software.

X-ray photoelectron spectroscopy (XPS). Figure 6 displayed the electron spectroscopy of synthesized TCA NC was examined by XPS analysis. A polymer TANI contains the carbon and nitrogen shown the respective peaks of phenyl C1s, C–C (Fig. 6b) and nitrogen containing aromatic polymers N1s (Fig. 6c) were centred at 284.8 and 399.7 eV. Besides that, the Cu and O in Cu_2O were observed at binding energy of 934.6 eV (Fig. 6d) for Cu $2p_{3/2}$, 955.02 eV for Cu $2p_{1/2}$ and 532.2 eV (Fig. 6e) respectively[33]. When compared to Ag°, a slight peak lower shift was observed in prepared Ag which is located at 367 and 372 eV are ascribed to $Ag3d_{5/2}$ and $Ag3d_{3/2}$ respectively, this may be due to disturb the chemical environment around Ag NPs in synthesized composite[34].

UV–visible/DRS spectroscopy. The UV–Visible absorption spectra of Cu_2O, TANI, TANI/Cu_2O and TCA NCs are shown in Fig. 7a. The UV–Visible absorption spectra of TANI, TANI/Cu_2O and TCA NCs show a peak at 326 nm which corresponds to π–π* transition of benzenoid ring of TANI[35]. Figure 7b (a–c) shows the optical bandgap energies of TANI, TANI/Cu_2O and TCA NCs obtained from the Eq. (1).

$$E_g = h\nu = hc/\lambda = 1240/\lambda \quad (1)$$

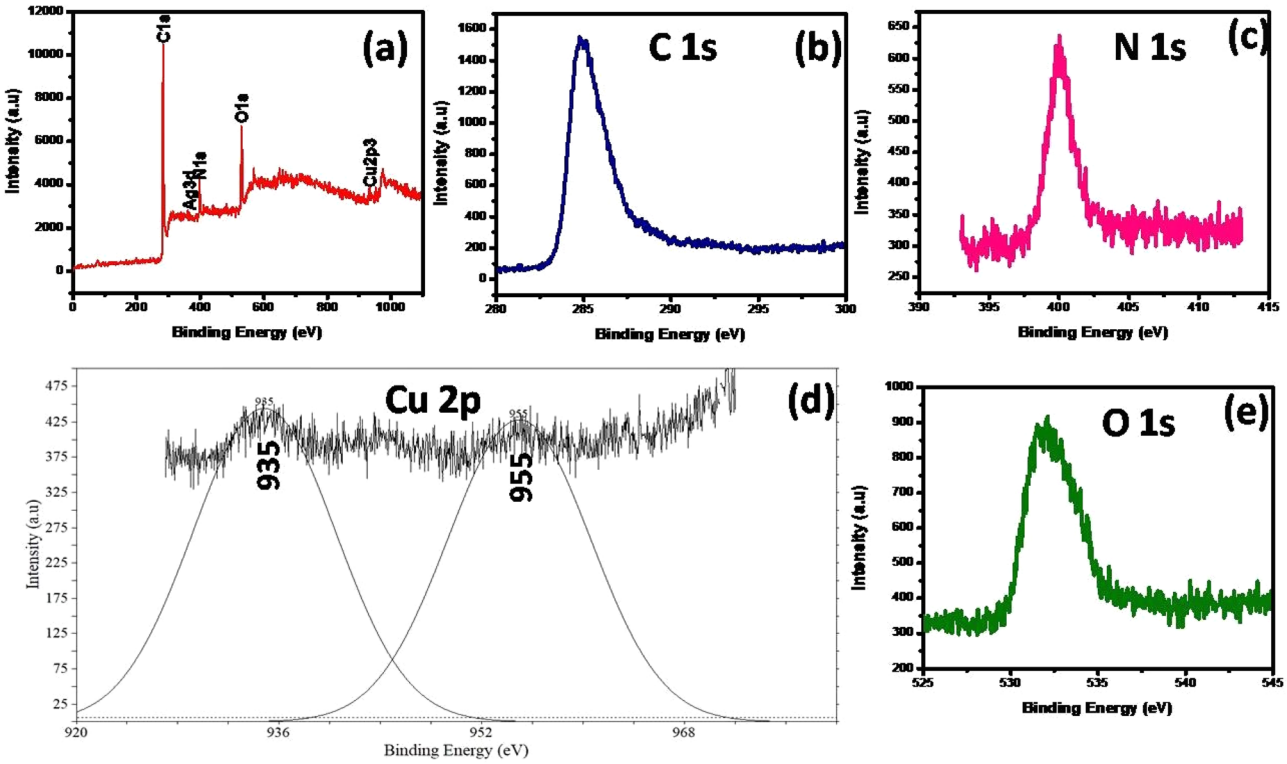

Figure 6. XPS analysis of (**a**) TCA NC, (**b**) C, (**c**) N, (**d**) Cu, and (**e**) O.

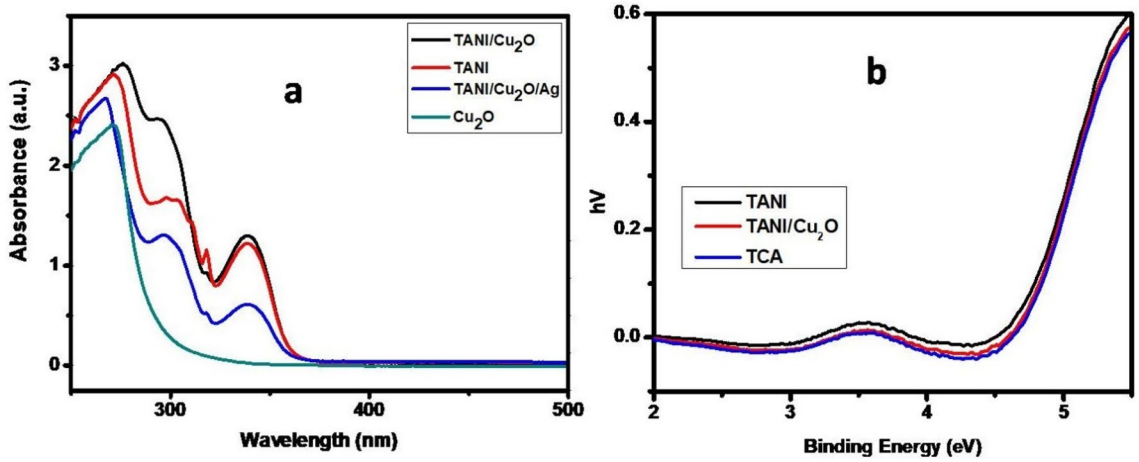

Figure 7. UV–Visible (**a**) absorption and (**b**) DRS spectra of prepared NCs.

where 'E_g' represents bandgap/forbidden energy, 'h' is plank's constant, 'υ' is wave frequency, 'c' is the speed of light and 'λ' is the wavelength.

Table S1 in ESI clearly stated that the somewhat decrease in bandgap energy of TCA NC ($E_g = 2.82$ eV) from pure TANI ($E_g = 2.93$ eV) due to embedded the p-type semiconductor, Cu_2O ($E_g = 1.98$ eV) into TANI matrix. The wider bandgap value originates from the quantum confinement effect which is caused by the nanodimensional state of materials. Lesser the bandgap materials possess excellence in catalytic activity, thus TCA NC has potent applications than other materials prepared.

Thermogravimetric (TG–DTA) analysis. Thermogram of the prepared NCs in an argon atmosphere as a carrier at a flow rate of 10 °C/min with a temperature range of 30–1,000 °C is depicted in Fig. 8a. The resultant graph implies the change in mass of the sample with increase in temperature. It was observed that pure TCA NC undergo three major steps of weight loss patterns but TANI and TANI/Cu_2O shows two major steps.

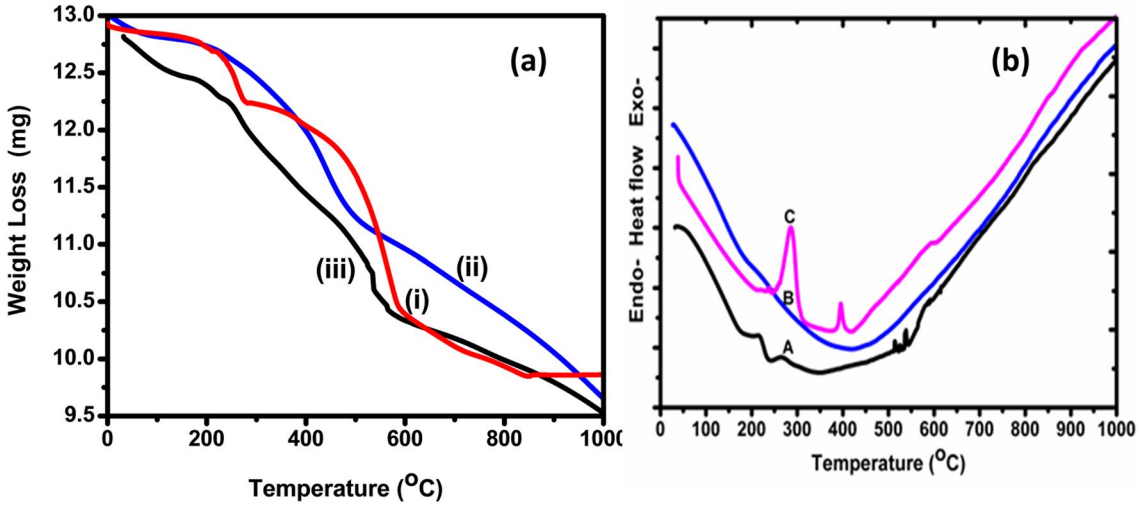

Figure 8. (**a**) Thermogram and (**b**) DTA curves of (**a**) pure TANI, (**b**) TANI/Cu_2O and (**c**) TANI/Cu_2O/Ag composites.

1. The first small fraction of weight loss in the temperature range from 30–270 °C is due to the loss of hydrate molecules from the surface of TANI and TCA NC held through weak ionic interactions[36].
2. The second major step of continuous weight loss occurs due to vanish the oligomers in TANI, TANI/Cu_2O and TCA NCs at the temperature range of 270–540°C[37].
3. Third step is decomposition process, shows a gradual weight loss occurs in the temperature range from 600–850 °C was observed due to thermal oxidative decomposition and degradation of the polymer fraction of TCA NC[38]. From the graph, it was seen that the thermal stability of TCA NC is considerably less than that of pure TANI and TANI/Cu_2O NC which shows high thermal stability. This may be due to decreased in chain length and the presence of bulky groups in the composites. This thermal stability was decreased in TCA NC is due to addition of Ag, may cause a decrease in the tension induced by thermal excitation in the C–C bond[39].

Figure 8b shows the DTA curves of pure TANI, TANI/Cu_2O and TCA NCs. This depict explored about thermal behaviour of composites from pure TANI. In Fig. 8b(C), the two exothermic peaks were observed at 280 and 420 °C, corresponding to their respective temperatures of polymer degradation and oxidation of NC. The oxidation at higher temperature means increase the content of Cu_2O in TCA composite and is evident from the Thermogram (Fig. 8a(C)). Figure 8b(B) shows the broad endothermic peak around the temperature of 440 °C, which corresponds to the decrease in degradation temperature of TANI/Cu_2O. Figure 8b(A) confirms the presence of exothermic peak at the temperature of 240 °C, corresponding to decomposed the TANI. These results tells about the interaction of Cu_2O and Ag NPs with polymers surfaces lead to formation of new compound of polymers which do not decompose into simple molecules such as carbon dioxide. The decrease in the degradation temperature of polymer nanocomposite to 280 °C, as compared to 240 °C of pure TANI, indicate that the polymers in the nanocomposite is different in its chemical nature compared to that in the pure state. However, the interpretation of the result needs further investigation.

Photoluminescence (PL) study. The photoluminescence spectra used not only to characterize the defects of a semiconductor but also to study the exciton spectra in TANI and its nanocomposites. Figure 9 illustrates the emission spectra of TANI and TCA NC at the excitation wavelength of 280 nm. In order to evidence the contribution of pure TANI and TCA NC shifted to 466 nm due to transitions from the polaronic band to the -band (HOMO) structures of TANI and the emission wavelength is shifted towards the blue when compared to the bulk TANI. This emission is due to the recombination of electron and hole pairs.

Catalytic applications of prepared nanomaterials. *Photocatalytic activity.* The photocatalytic activities of TANI, Cu_2O, TANI/Cu_2O and TCA NCs were studied by selective organic pollutant pararosaniline (PRA) dye under visible light irradiation at normalized conditions such as dye concentration (10 mg/L), pH (11) and catalyst dose (30 mg). The characteristic absorption of PRA dye solution at the wavelength ($\lambda = 545$ nm) used to monitor the photocatalytic degradation process. Figure 10a–d shows the UV–Vis absorption spectra of PRA dye solutions by TANI, Cu_2O, TANI/Cu_2O and TCA composites for 90 min. These results declared that the deep green colour of the initial PRA solution gradually fades to colourless during the process of photodegradation as the exposure time is extended. Figure 10a shows the photocatalytic activity of TANI, clears that no significant photodegradation (11%) of PRA dye. Figure 10b shows the photocatalytic activity of Cu_2O, stated that the dye was degraded partially (59%) due to faster recombination rate of electron and hole pair. Therefore, further, the binary composite TANI/ Cu_2O was tested under same conditions and shows (Fig. 10c) the excellent photocatalytic activity (85%). So as to complete photodegradation of PRA dye, both Cu_2O and Ag were fabricated onto

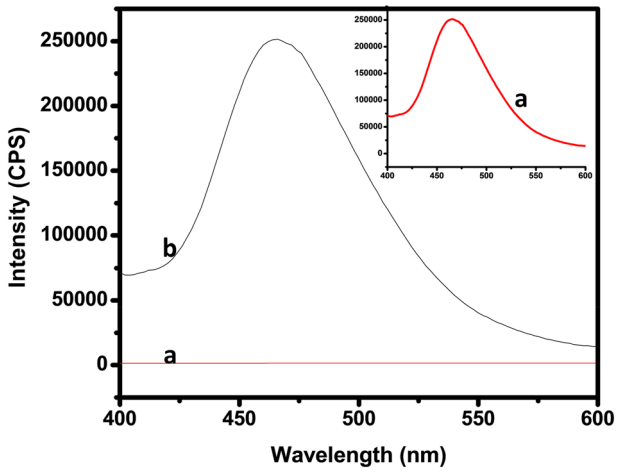

Figure 9. PL spectra of (**a**) TANI/Cu_2O/Ag NC and (**b**) pure TANI.

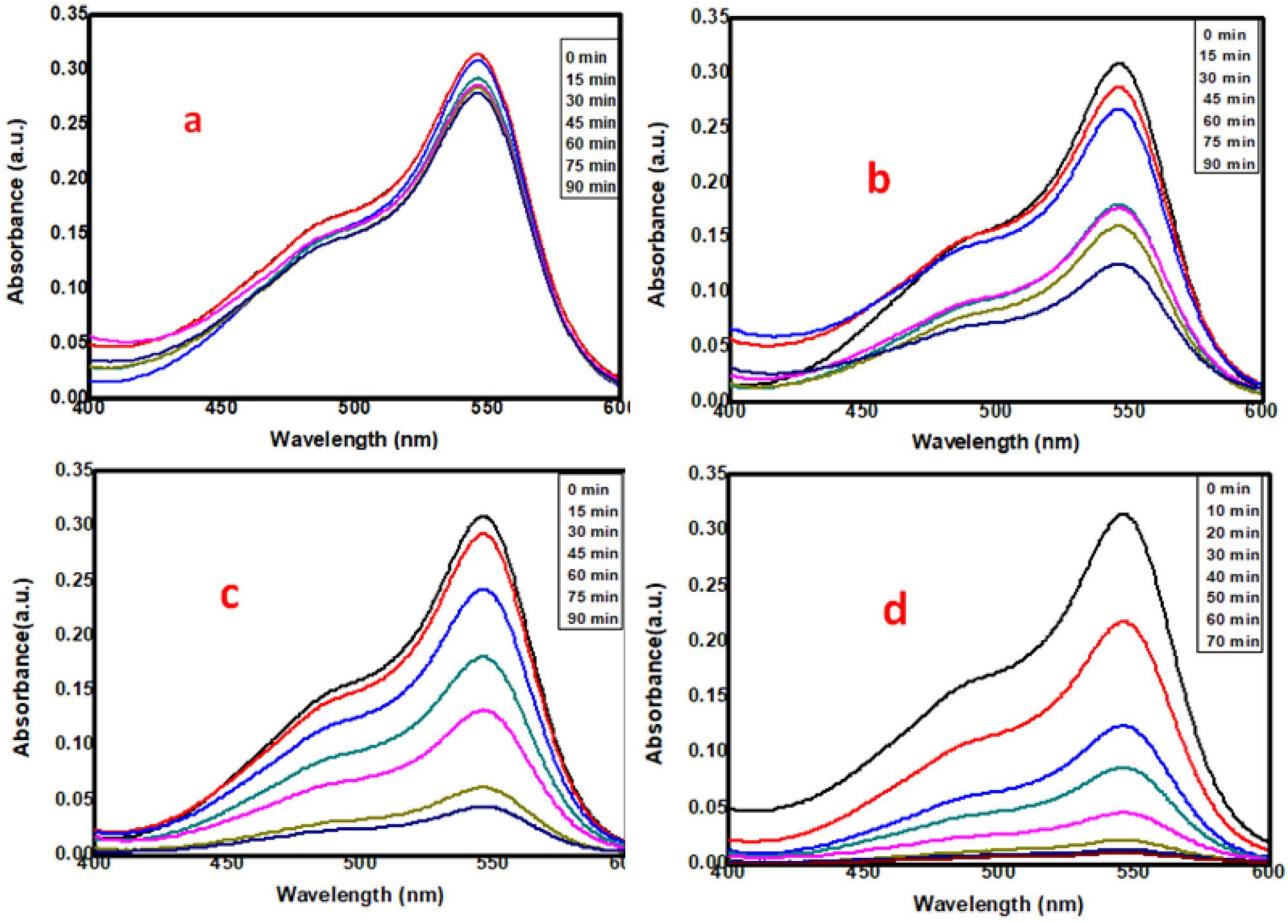

Figure 10. Photocatalytic activity of (**a**) TANI (**b**) Cu_2O (**c**) TANI/Cu_2O and (**d**) TANI/Cu_2O/Ag.

TANI matrix. This ternary composite was nearly complete degraded (97%) the PRA dye (Fig. 10d) under visible light illumination in 70 min due to Ag plays an important role in photocatalysis as it entrant electrons and reduce the gap between electron and hole pair. For instance, the Ag NPs in Ag/Ag_2O act as sink for the photogenerated electrons and contribute a great role in the phenol degradation process by preventing electron–hole recombination with holes[40]. It indicates that the ternary nanocomposite has high photostability towards the degradation of PRA under visible light illumination (Fig S2(a) in ESI). The target molecule PRA is relatively stable in aqueous solutions under visible light illumination.

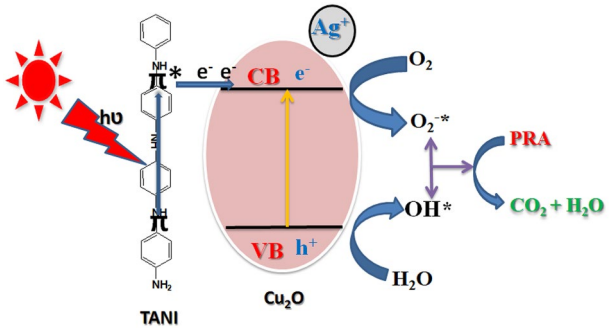

Figure 11. A plausible mechanism for dye degradation by TANI/Cu_2O/Ag NC.

In addition, the rate order kinetics of prepared composites calculated using Eq. (2), according to the Langmuir–Hinshelwood kinetics model, the function of $\ln(C/C_0)$ versus reaction time (t) displayed a linear relationship as show in ESI (Fig S2b).

$$\ln C/C_0 = kt \tag{2}$$

where 'C/C_0' is normalized initial concentration, 't' is the reaction time, and 'k' is the reaction rate constant (min^{-1}). The corresponding pseudo first order kinetic rate constant (k) and regression coefficient (R^2) of PRA were calculated and are listed in the Table S2 (ESI). These results confirmed that all are follows the pseudo first order rate.

Proposed mechanism. Proposed a plausible mechanism for improved the photocatalytic degradation efficiency of TANI/Cu_2O/Ag ternary nanocomposite in the presence of visible light irradiation was displayed in schematic diagram Fig. 11. Initially, TANI was kept in visible light illumination, $\pi \rightarrow \pi^*$ transition takes place, which release the electrons Eq. (5). In similar way, Cu_2O undergoes charge separation process that leads to the promotion of electrons from valence band (VB) to conduction band (CB) and leaving a hole in the VB and releasing of electrons Eqs. (6, 7) due to the formation of heterojunction. Ag reduced and resulting in release of electrons Eq. (8). Finally, the photogenerated electrons are captured by the TANI through semiconductor Cu_2O due to heterojunction which helps in enhancing the photogenerated charge separation efficiency in ternary nanocomposite. Simultaneously an equal amount of holes have been formed in semiconductor nanocomposite. These separated electrons and holes directly reacts with oxygen and water to generate highly reactive superoxide ($^{\cdot}O_2^-$) and hydroxyl ($^{\cdot}OH$) radicals Eq. (9). These energetic reactive radicals react with surface adsorbed PRA molecules and degraded them into CO_2 and H_2O Eq. (10).

Based on this mechanism, explained the photocatalytic degradation of PRA dye using TCA nanocomposite under visible light irradiation as shown by the following Eqs. (3–8).

$$\mathrm{TANI}(\pi) + h\nu \rightarrow \mathrm{TANI}(\pi^*) + \mathrm{TANI}(e^-) \tag{3}$$

$$Cu_2O(h^+) + H_2O \rightarrow Cu_2O + {}^{\cdot}OH + H^+ \tag{4}$$

$$Cu_2O(e^-) + O_2 \rightarrow Cu_2O + {}^{\cdot}O_2^- \tag{5}$$

$$Ag \rightarrow Ag^+ + e^- \tag{6}$$

$$\mathrm{TANI/Cu_2O/Ag}(e^-) + O_2 \rightarrow \mathrm{TANI/Cu_2O/Ag} + {}^{\cdot}O_2^- \tag{7}$$

$$^{\cdot}OH/^{\cdot}O_2^-/HO_2^{\cdot} + \mathrm{PRA\ dye} \rightarrow \mathrm{Degradation\ products} \tag{8}$$

Based on experimental conditions, TCA ternary nanocomposite possesses high photocatalytic activity towards the degradation of PRA dye solution under visible light irradiation than the binary composite and pure TANI.

Radical affirmation by Scavenger test. In order to endorse the radicals scavenging, initially the 10 mg/L PRA dye solution was taken along with 30 mg TCA NC allowed to irradiation for 70 min in the presence of scavengers such as tertiary butyl alcohol (t-BuOH), Benzoquinone (BQ) for OH, O_2^-, and potassium iodide (KI) for hole and OH radical. Remarkably, the absence of scavenger has shown better results almost 96.3% of PRA dye suspension yet, when used scavengers declined the removal percentage like KI-40.9%, BQ-44.5%, t-BuOH-42.7% as presented in ESI (Fig S3).

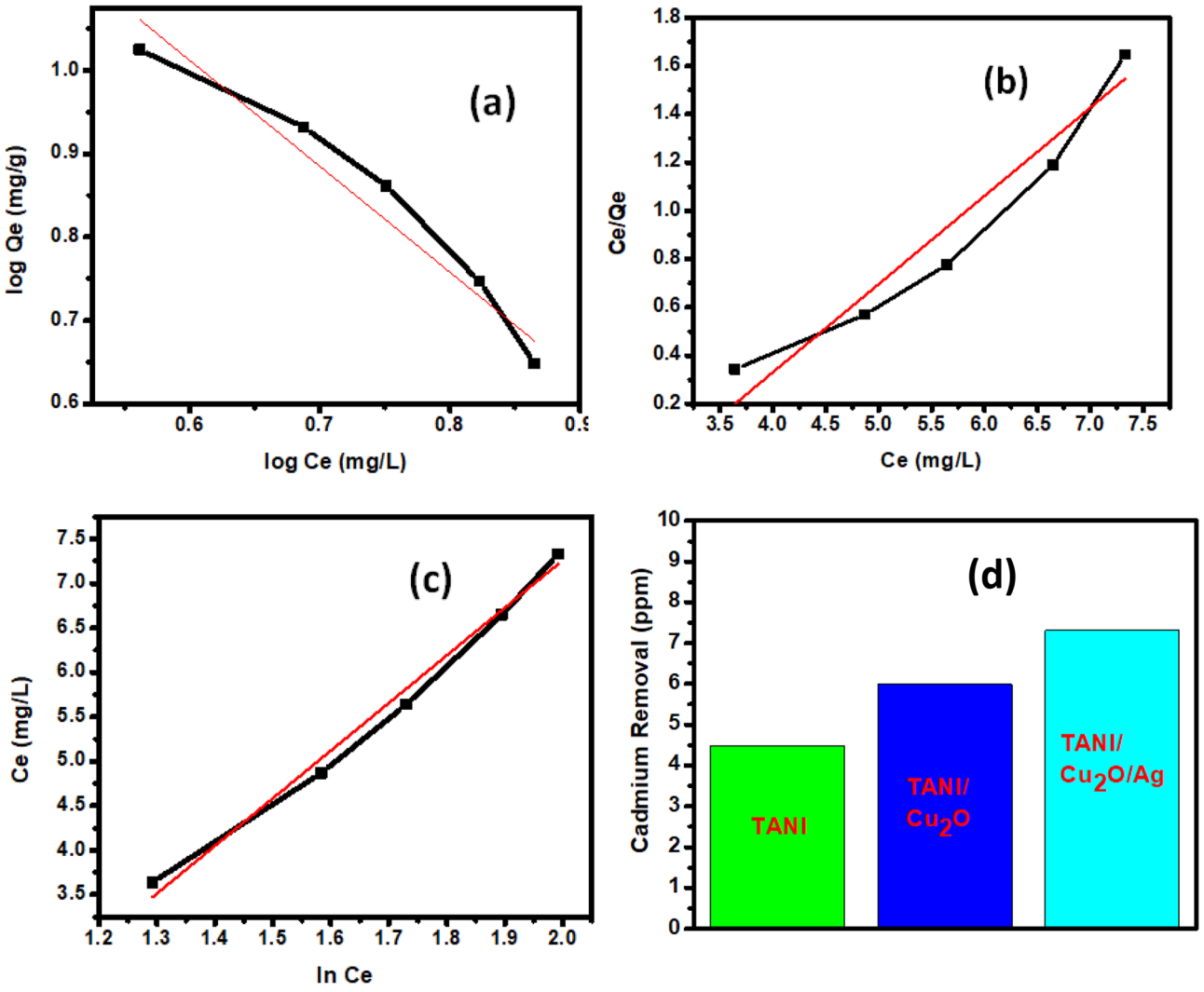

Figure 12. Adsorption isotherms of (**a**) Freundlinch, (**b**) Langmuir, (**c**) Temkin and (**d**) removal of Cd^{2+} (mg/L) by prepared materials.

Stability and recycling of TCA composite. In favour of investigate the reusability of synthesized TCA composite, the synthesized TCA was cleaned with milli Q water followed by ethanol and centrifuged to execute the later reaction. Significantly, the photodegradation of PRA dye is declined gradually up to five successive runs as 97, 96.1, 95.2, 94 and 92.7% for the successive five cycles respectively. This may be due to the loss of TCA during washing for recyclability. Fig S4(a) in ESI stated that prepared TCA composite acted as very dynamic photocatalyst up to five successive runs, thus the TCA photocatalyst remains stable and potent because of the presence of TANI surface to $Cu_2O$and Ag in synthesized composite that leads to mobilize the photogenerated electron and holes, so enhance the photocatalytic efficacy[41]. Fig S4(b) in ESI implies the XRD patterns of TCA which confirmed that no phase change was noticed in recycled TCA composite after reusable for successive five runs. From the obtained results, we strongly declared that polymerization synthesized TCA nanocomposite can be probably used as a stable photocatalyst for the dye (PRA) degradation in large scale.

Removal of cadmium ion (Cd^{2+}) by adsorption. The prepared pure TANI and their composites (TANI/Cu_2O and TCA) were studied the adsorption efficiency by the removal of cadmium (Cd^{2+}) from contaminated water under the conditions of catalyst dose 30 mg and Cd^{2+} solution 10 mg/L in alkaline medium. The obtained results declared the ternary composite shows better adsorption (7.5 mg/L) of Cd^{2+} than binary TANI/Cu_2O (6 mg/L) and TANI (4.5 mg/L) owing to the presence of Cu_2O and Ag NPs into TANI matrix are displayed in Fig. 12. However, the polymer based composite exhibits more adsorption capacity due to the presence of more surface groups, greater adsorption capacity, good stability and mechanic viability[42]. In this study, three most common isotherms such as Freundlich, Langmuir and Temkin models are used to interpret the experimental adsorption data. The equilibrium adsorption isotherms were determined using batch studies.

Model	R^2	Intercept	Slope
Freudnlinch	0.94001	1.77388	1.26974
Langmuir	0.93305	1.13018	0.36536
Temkin	0.98716	3.44367	5.35335

Table 1. Rate order kinetics for adsorption isotherm models.

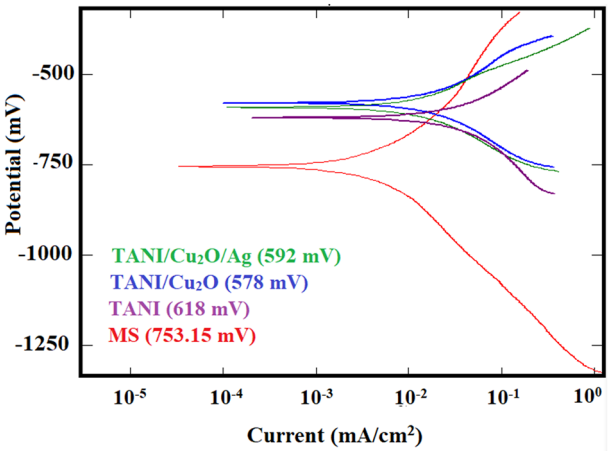

Figure 13. Corrosion Inhibition plot of as-prepared composites.

Freundlich model. According to Freundlich equation, the amount adsorbed increases infinitely with increasing concentration or pressure. The Freundlich Eq. (9) isotherm can be linearized into the following form:

$$\log Q_e = \log k_F + 1/n \log C_e \tag{9}$$

The regression coefficient (R^2), slope and intercept were 0.94, 1.26 and 1.77 respectively. From these results, n and k_F values were calculated to be 0.78 and 58.41 respectively (Fig. 12a).

Langmuir model. Langmuir isotherm Eq. (10) is derived from simple mass kinetics, assuming chemisorption. This model was depicted in Fig. 12b. From this graph, calculated the regression coefficient (R^2), slope and intercept were 0.93, 0.36 and − 1.13 respectively. From these results, Q_{max} and k_L are 2.73 and 0.32 respectively, desorption of the Cd^{2+} is very low.

$$C_e/Q_e = 1/k_L Q_{max} + C_e/Q_{max} \tag{10}$$

Temkin model. The linear relationship can be calculated from Eq. (11) and the result was depicted in Fig. 12c. The regression coefficient (R^2), slope and intercept were calculated to be 0.98, 5.35 and − 3.44 respectively. The adsorption capacity and adsorption intensities, Q_e and ln k_T; 5.9 and 0.63 respectively obtained.

$$Q_e = B_1 \ln k_T + B_1 \ln C_e \tag{11}$$

From these results, the Freundlich model was fitted for the adsorption of Cd^{2+} onto ternary nanocomposite (Table 1).

Corrosion inhibition. The corrosion resistance behaviour of synthesized pure TANI, TANI/Cu_2O and TANI/Cu_2O/Ag composite coatings were evaluated by sweeping the potential from equilibrium potential towards negative and positive potentials against Ag/AgCl reference electrode in H_2SO_4 (1 M), HCl (1 M) and NaCl (3.5%, w/w) electrolytes using Tafel polarisation and electrochemical impedance spectroscopy techniques (Fig. 13). The trends of open-circuit potential curves provided clear evidence that the incorporation of Cu_2O into TANI nanostructures is beneficial, as it introduces potential shift towards the noble positive potential for both binary and ternary composite coatings. But the ternary composite doesn't show the good corrosive resistance behaviour than binary composite because of low percent of Ag content in composite, which doesn't shows the adverse effect on corrosion inhibition. Also, the corrosion resistance was enhanced with increase in the Cu_2O content in TANI supported nanocomposite coatings. Table 2 displays the values related to the corrosion current (I_{corr}), corrosion potential (E_{corr}), cathodic (β_a), anodic (β_c) slopes and corrosion rate (CR) were calculated from tafel plots for pure TANI, TANI/Cu_2O and TANI/Cu_2O/Ag nanocomposites, also their polarization resistance (R_p) was calculated from kinetic parameters obtained from Tafel plots as Stern–Geary Eq. [43].

Specimen	E_{corr} (mA/cm²)	I_{corr} (mA/cm²)	β_a (mV)	β_c (mV)	Corrosion rate (mm/year)
TANI	−652.46	0.07676	181.87	176.67	0.89
TANI/Cu_2O	−441.52	0.06121	196.16	517.53	0.71
TANI/Cu_2O/Ag	−616.03	0.0706	167.05	158.39	0.80

Table 2. Electrochemical parameters estimated from potentiodynamic polarization curves.

$$R_p = \frac{\beta_a \times \beta_c}{2.303} \times I_{corr}(\beta_a + \beta_c) \quad (12)$$

where β_a and β_c are the respective slopes of cathodic and anodic tafel plots. Fig S5 (ESI) represents the bar graph which declared that TANI/Cu_2O binary composite has high intensity in corrosion inhibition than TANI/Cu_2O/Ag ternary composite and pure TANI was confirmed by the values of binary composite goes towards positive of E_{corr}, with the comparison of mild steel (MS) as reference. The Tafel polarization studies showed the decreased corrosion current for all the TANI/Cu_2O composite coatings than TANI/Cu_2O/Ag and TANI. Hence, the corrosion inhibition rate of TANI/Cu_2O nanocomposite coatings is less than that of TANI/Cu_2O/Ag. It is revealed that TANI/Cu_2O nanocomposite had more corrosion resistant in 3.5% NaCl solution.

Antibacterial assay. The antibacterial activity of as-prepared nanocomposites was tested on four different micro-organisms. For that, initially we examined with the all prepared compounds, of them, only binary and ternary nanocomposites showed better antimicrobial efficacy. Hence based on the results, further studies were on TANI/Cu_2O and TANI/Cu_2O/Ag NCs against the both gram negative (*Shigella flexneri*, *Salmonella* typhimurium) and gram positive (*Bacillus coagulans*, *Staphylococcus aureus*) bacterial strains at three consecutive concentrations of 40, 60 and 80 µg/mL.

Antimicrobial assay of TANI/Cu_2O nanocomposite. Finally, the antimicrobial activity of TANI/Cu_2ONC was executed against the four different pathogens including gram positive and negative bacteria. Figure S6 displays the photographic images of an inhibition zone was rendered by TANI/Cu_2ONC against four different bacterial strains. The zone of inhibition of TANI/Cu_2ONC for various microorganisms is shown in Table S3 (ESI). Among all the strains selected for this study, *S.aureus is* the most active strain (21 µg/mL) at the concentration of 80 µg/mL. The synthesized TANI/Cu_2ONC is effectively inhibited the bacterial growth and gram positive (*S.aureus)* is observed to be so effective than gram negative (*S. typhimurium)* bacteria.

Antimicrobial activity of TANI/Cu_2O/Ag nanocomposite. The TANI/Cu_2O/Ag NC was tested against the both gram positive and gram negative bacterial strains. Figure 14 shows the photographic images of an inhibition zone produced by TCA NC against four different bacterial strains. The zone of inhibition of TCA NC for various microorganisms was shown in Table 3. The influence TCA NC on *S. aureus* (25 µg/mL) and *S.typhimurium* (22 µg/mL) exhibited the best results at the examined concentration of 80 µg/mL. The prepared TCA NC effectively killing the bacterial growth and gram positive is observed to be so might effective than gram negative bacteria.

The significant antimicrobial activity was not found by pure TANI and Cu_2O. The binary and ternary composites show antimicrobial efficiency against both Gram-positive and negative bacteria. These results proposed two different mechanisms of ternary composite with target microorganism interaction, the first: adsorption of ternary composite to cell walls, membrane disruption and cell leakage which is mainly connected with high molecular weight ternary composite, the second: penetration of ternary composite into living cells leading to inhibition of various enzymes and interference with synthesis of mRNA and proteins. However, the actual mechanism of inhibition activity of TANI/Cu_2O/Ag composite is not fully understood yet.

In present study, the antimicrobial performance confirmed that gram positive bacterial strains are more affected than gram negative (Fig S7) because Gram positive bacteria have thin peptidoglycan layer with abundant pores that permits foreign molecules to penetrate into cell and damage or malfunctioning the cell organisms. Gram positive and gram negative bacteria have differences in their membrane structure, the most distinctive of which is the thickness of the peptidoglycan layer. The high concentration of Cu^0 affected bactericidal effect. Therefore, copper nanoparticles are chosen as a carrier in this work[44]. A very few reports on Ag ions effects on microorganisms in which Ag^+ attracts the negatively charged cell membrane of microorganism through electrostatic interactions[45]. Hence, Ag^+ plays a vital role in the antibacterial activity of Ag in solutions with salts, zeolites and polymers[46]. For instance, the AgNP-polymeric nanoparticles showed increased antimicrobial properties towards *E.coli* and *S.aureus*[47]. The Ag NPs induced oxidative stress on bacteria and also damaged the cell membrane, protein, and DNA[48]. However, the Ag NPs can be easily penetrate to cell wall of microorganisms and also their greater surface area enhance the antimicrobial performance by bring a huge atoms into intact with the parts of bacteria[47]. Hence, the Ag NPs were used in the study, however, they received negative charge from TANI. The biological activity of Ag and Cu nanoparticles is also dependent on their size, causing penetration and damage of Gram-positive and negative bacteria cells[49]. The mechanism of the inhibitory effects of ternary composite on microorganisms is not yet known clearly. Further investigation was required.

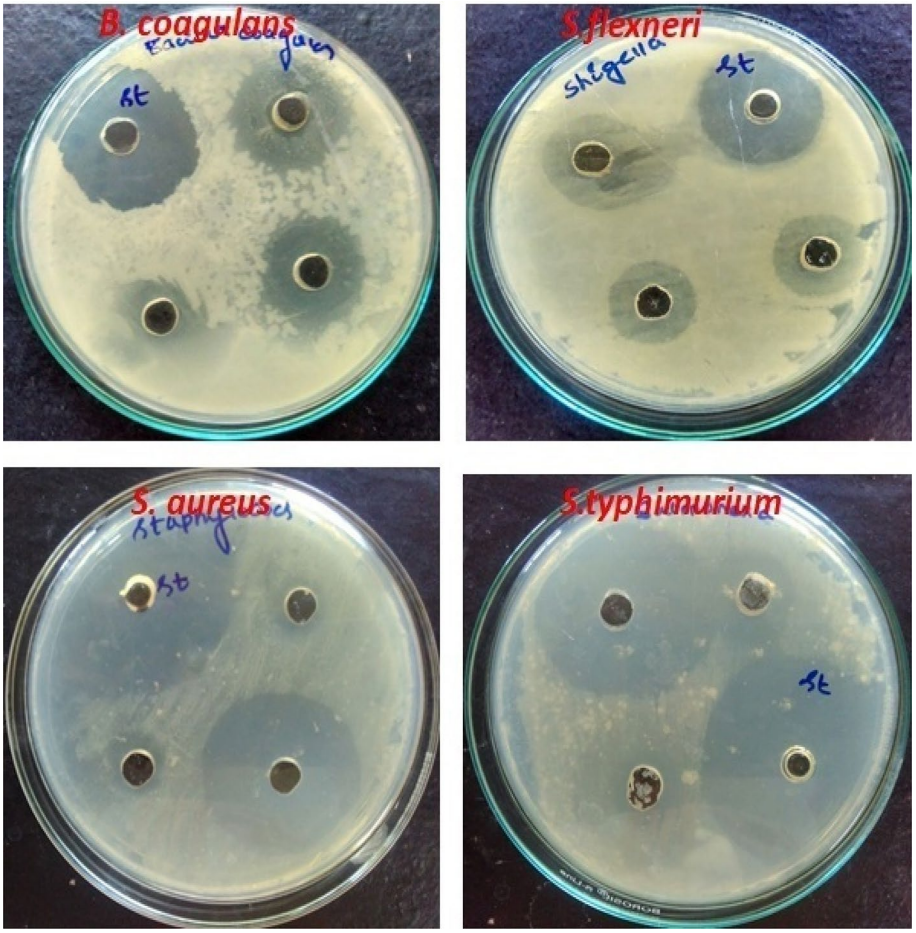

Figure 14. Antimicrobial activity of TANI/Cu_2O/Ag NC.

S. nos.	Organism	Zone of inhibition (mm)			
		40 µg/mL	60 µg/mL	80 µg/mL	Standard (chloramphenicol) 30 µg/mL
1	*Bacillus coagulans*	16	19	20	22
2	*Shigellaflexneri*	15	16	18	20
3	*Staphylococcus aureus*	10	12	25	25
4	*Salmonella typhimurium*	12	18	22	26

Table 3. The zone of inhibition of TANI/Cu_2O/Ag NC.

Conclusion

In this work, a facile, simple and *insitu*-polymerisation approach is developed to obtain novel TANI/Cu_2O/Ag ternary nanocomposite. On the basis of the result of UV – Vis spectra, electron density on Ag NPs results in a bathochromic shift of SPR peak of Ag NPs. Thermogram of TANI/Cu_2O/Ag NC undergo three steps of weight loss patterns. The ternary nanocomposite was tested photocatalytic, adsorption, corrosion and antibacterial activity. It acts as benign eco-friendly material towards water treatment. It exhibits good photocatalytic activity by the complete degradation of pararosaniline (PRA) dye under visible light irradiation in 70 min. Similarly, this composite acted as good sorbent for 590 mg/g of cadmium (Cd^{2+}) in 90 min. But, corrosion was inhibited more by the synthesized TANI/Cu_2O composite than as expected TCA NC due to E_{corr} values shift towards positive and this is may be does not show any effect by Ag. TANI/Cu_2O/Ag acts as potent and shows enhanced antimicrobial agent against both gram positive and negative bacteria. The ternary nanocomposite shows excellent catalytic properties than binary composite and pure TANI except for anti-corrosion.

Experimental section

Materials. Copper acetate monohydrate $Cu(CH_3COO)_2\ H_2O$, sodium hydroxide NaOH, hydrazine hydrate $N_2H_4\ H_2O$, N-phenyl-1,4-phenylediamine (NPPD), sodium chloride NaCl, hydrochloric acid HCl and silver nitrate $AgNO_3$ were procured from Sigma aldrich, India. Cadmium nitrate $Cd(NO_3)_2$ and toluene were received from Merck chemicals, India. Analytical grade chemicals were utilized same as received without further purification. Throughout all synthesis process doubled distil water used.

Synthesis of Cu_2O Nps. For the preparation of Cu_2O Nps[7], initially 100 mL of 0.25 M $Cu(CH_3COO)_2\ H_2O$ was ultrasonicated for 10 min, then added 100 mL of 0.1 M NaOH to the above solution. The mixture solution further ultrasonicated for 20 min, followed by adding of 1.2 mL hydrazine hydrate drop wisely and continued the ultrasonic irradiation for 30 min at ambient air. The ultrasonic irradiation was generated with a high intensity ultrasonic probe (Vibracell sonics, Ti-horn, 1.1 cm diameter, 20 kHz, 50% amplitude, 60 W/cm^2) dipped in the reaction vessel. During the reaction, almost 50 °C temperature was recorded as not used any cooling. The reddish precipitate was formed, which is centrifuged, washed with Milli Q water and absolute ethanol in sequence, finally dried at 60 °C in hot air oven to obtain the pure Cu_2O nanoparticles.

Simultaneous synthesis of TANI/Cu_2O/Ag ternary nanocomposite. In typical synthesis process, equimolar (0.01 M) of aqueous APS (adding of 10 mL 1 N HCl) and $AgNO_3$ solutions were prepared with same molar of NPPD solution was prepared with toluene; as prepared 25 mL of aqueous $AgNO_3$ and APS solutions were carefully added to 50 mL of NPPD solution in 250 ml beaker and then the reaction was allowed to room temperature. The aqueous phase of the solution turns into light green colour within 30 min and gradually turns into dark green colour. The beaker kept in dark room for 12 h. Then separated the aqueous phase and centrifuged. Discarded the supernatant liquid and periodical washing has been done with acetone and water. Finally the product (TANI/Cu_2O/Ag) was dried under vacuum at room temperature. This procedure has been same for the preparation of TANI/Cu_2O without adding of $AgNO_3$ solution. Similarly, pure TANI was synthesized in the absence of both Cu_2O and $AgNO_3$ solution.

Characterization. The diffraction peaks were recorded by powder X-Ray diffraction (XRD D8 Bruker AXS) with Cu-Kα radiation at 30.0 kV and 30.0 mA over the scan range (2θ) 10–90° at the scan rate of 2°/min. FTIR (IR Prestige21, Shimadzu Pvt Ltd, Japan) spectra of the samples in KBr pellets were obtained on a Shimadzu spectrometer in the range of 400–4,000 cm^{-1}. Morphology of the prepared materials was investigated by Scanning electron microscopy (FESEM, JSM-6610LV, Jeol Asia PTE Ltd, Japan.) and the elemental analysis was done by EDS. UV–Visible absorption and diffuse reflectance spectra were recorded by UV–Visible diffuse reflectance spectrometer (Shimadzu 2600R) in the range of 200–800 nm. The PL spectra of prepared composite were taken using Flouromax-4, HORIBA, Japan to elucidate the transfer behaviour of photo-induced electrons and holes. X-ray photoelectron spectroscopy (XPS) spectra obtained from Physical electronics PHI 5,000 versaprobe III with C60 ion gun to study the electron spectroscopy of TCA composite.

Photocatalytic studies. The photocatalytic performances of produced samples were conducted. The suspensions for the photocatalytic reaction were prepared by adding 0.03 g of various catalysts to a required concentration of dye and pollutant solutions. Before illumination, the mixture was magnetically stirred for 30 min in the dark to establish adsorption–desorption equilibrium of organic pollutants with the catalyst. A solar simulator with a metal halide lamp was used as the visible light source. The experimental solution was placed in a quartz cuvette, 100 mm away from the light source. 5 mL of the suspension was withdrawn at regular time intervals and centrifuged to remove the dispersed catalyst powder. The concentration of the clear solution was determined using UV–Visible absorption spectra. The photodegradation efficiency was determined by measuring the absorbance spectra of the dye solution before (C_0) and after the photocatalytic reaction with variation of time (C_t). The degradation efficiency of the photocatalytic reaction was calculated using Eq. (13)

$$\text{Degradation efficiency (DE\%)} = \frac{C_0 - C_t}{C_0} = \frac{A_0 - A_t}{A_0} \times 100 \tag{13}$$

where C_0 or A_0 are initial concentration or absorbance and C_t or A_t after the photocatalytic reaction concentration or absorbance with various time (t).

Adsorption studies. The deletion of heavy metals like cadmium ions (Cd^{2+}) via adsorption process by *insitu* polymerisation synthesized nanocomposite. During this process, 0.03 g of the sorbent was added to 10 mg/L of Cd^{2+} solution under stirring for 90 min in dark condition. Then, gathered the solution mixture at every 15 min time intervals which were further analysed by UV–Visible spectrophotometer. The amount of Cd^{2+} adsorbed onto the ternary composite can be calculated by the mass balance relationship by the following Eq. (14).

$$\text{Adsorption capacity } \left(\text{mg/g}\right),\ q_e = (C_o - C_e)/W \times V \tag{14}$$

where w is the weight of the adsorbent (g), and V is the volume of the solution (L).

Inhibition of corrosion analysis. The anticorrosion activity of as-prepared samples has been analysed for pitting corrosion and the test conducted through potentiodynamic polarization procedure using software based PAR weld electrochemical system of the GILL AC unit with the sample dimensions of 20 × 20 × 10 mm. A satu-

rated calomel electrode and carbon electrode were used as reference and auxiliary electrodes respectively. All the experiments were piloted in aerated 3.5% NaCl solution with pH adjusted to 10 by adding potassium hydroxide. The exposure area for these experiments was 1 cm^2 and current has been inducted into an electrolyte. The pitting corrosion resistance of the samples has been determined by obtained E_{corr} values, which is current equal to the potential at anode and cathode.

Inhibition of bacterial growth assay. The synthesized TANI and its binary and ternary nanocomposites were tested for antibacterial activity over the bacterial strains of Salmonella typhimurium (MTCC-3231).

Shigella flexneri (MTCC-1457), *Bacillus coagulans* (MTCC-5856) and *Staphylococcus aureus* (MTCC-3160) grown overnight at 37 °C temperature and the medium was sterilized by autoclaving at120 °C (15 lb/in^2). The nutrient agar medium, 20 mL with the respective bacterial strains of bacteria were transferred aseptically into each sterilized Petri plate, which were allowed to cool at room temperature for solidification. Each plate was made into 5 wells with equal distance of 6 mm sterile borer. Chloramphenicol was taken as positive control for bacterial species. The antibacterial activity of the compound was evaluated by well-established Agar well diffusion method. The four wells were made and filled with concentrations of 40, 60 and 80 μg/mL of tested samples and then plates were incubated for a period of 24 h at 37 °C in incubator, after incubation the inhibitory zone formed around the well was measured.

Data availability

The data was generated and analyzed during the current study are available from the corresponding author on reasonable request.

Received: 29 October 2019; Accepted: 21 June 2020
Published online: 21 August 2020

References

1. Speidel, E. D. H., Ruedisili, L. C. & Agnew, A. F. *Perspectives on Water Uses and Abuses* (Oxford University Press, New York, 1988).
2. United State Environmental Protection Agency (EPA). The National Water Quality Inventory: Report to Congress for the 2002 Reporting Cycle—a Profile, Washington DC. Facts Sheet No. EPA 841-F-07- 03 (2007).
3. Lagaly, G. Pesticide–clay inte ractions and formulations. *Appl. Clay Sci.* **18**, 205–209 (2001).
4. Fan, Z., Yue-Hua, L., Jing-Yu, L., Zi-Rong, T. & Yi-Jun, X. 3D graphene-based gel photocatalysts for environmental pollutants degradation. *Environ. Pollut.* **253**, 365–376 (2019).
5. Xin, S. *et al.* Electricity generation and microbial community of single-chamber microbial fuel cells in response to Cu_2O nanoparticles/reduced graphene oxide as cathode catalyst. *Chem. Eng. J.* **380**, 122446 (2020).
6. Cheng, M. *et al.* Hydroxyl radicals based advanced oxidation processes (AOPs) for remediation of soils contaminated with organic compounds: a review. *Chem. Eng. J.* **284**, 582–598 (2016).
7. Botsa, S. M. & Basavaiah, K. Removal of Nitrophenols from wastewater by monoclinic CuO/RGO nanocomposite. *Nanotechnol. Environ. Eng.* **4**, 1 (2019).
8. Khin, M. M., Nair, A. S., Babu, V. J., Murugan, R. & Ramakrishna, S. *Energy Environ. Sci.* **5**(8), 8075–8109 (2012).
9. Mohan, B. S., Ravi, K., Sree, G. S., Anjaneyulu, R. B. & Basavaiah, K. Fe_2O_3/RGO nanocomposite photocatalyst: Effective degradation of 4-Nitrophenol. *Phy. B Condens. Matter.* **556**, 190–194 (2019).
10. Nan, Z., Min, Q., Yang, S. L., Yugang, S. & Yi-Jun, X. Waltzing with the versatile platform of graphene to synthesize composite photocatalysts. *Chem. Rev.* **115**(18), 10307–10377 (2015).
11. Sunkara, J. R. & Botsa, S. M. SnO_2/Fe_2O_3/Ag nanocomposite via hydrothermal approach: a novel highly efficient photodegradation of eosin yellow and brilliant green dyes under visible light irradiation. *Chem. Afr.* **2**, 635–644 (2019).
12. Kurian, M. & Nair, D. S. Heterogeneous Fenton behavior of nano nickel zinc ferrite catalysts in the degradation of 4-chlorophenol from water under neutral conditions. *J. Water Process. Eng.* **8**, 37–49 (2015).
13. Botsa, S. M. & Basavaiah, K. Sonochemical assisted synthesis of CuO for degradation of nitrobenzene under visible light irradiation and antimicrobial activity. *J Nanosci. Technol.* **4**(5), 467–470 (2018).
14. Botsa, S. M., Dharmasoth, R. & Basavaiah, K. A facile synthesis of Cu_2O and CuO nanoparticles via sonochemical assisted method. *Curr. Nanosci.* **2**, 209–213 (2019).
15. Heeger, A. J. Semiconducting and metallic polymers: the fourth generation of polymeric materials. *Angew. Chem.* **40**, 2591–2611 (2001).
16. MacDiarmid, A. G. Synthetic metals: a novel role for organic polymers. *Angew. Chem.* **40**, 2581–2590 (2001).
17. Lee, K. *et al.* Metallic transport in polyaniline. *Nature* **441**, 65–68 (2006).
18. Yusoff, A. R. B. M. & Shuib, S. A. Metal-base transistor based on simple polyaniline electropolymerization. *Electrochim. Acta.* **58**, 417–421 (2011).
19. Bejbouj, H. *et al.* Influence of the nature of polyaniline-based hole-injecting layer on polymer light emitting diode performances. *Mater. Sci. Eng B.* **166**, 185–189 (2010).
20. Zhang, K., Zhang, L. L., Zhao, X. S. & Wu, J. S. Graphene/polyaniline nanofiber composites as supercapacitor electrodes. *Chem. Mater.* **22**, 1392–1401 (2010).
21. Bejbouj, H. *et al.* Polyaniline as a hole injection layer on organic photovoltaic cells. *Sol. Energy Mater. Sol. Cells.* **94**, 176–181 (2010).
22. Arshak, K., Velusamy, V., Korostynska, O., Oliwa-Stasiak, K. & Adley, C. Conducting polymers and their applications to biosensors: emphasizing on foodborne pathogen detection. *IEEE Sens. J.* **9**, 1942–1951 (2009).
23. Nemzer, L. R., Schwartz, A. & Epstein, A. J. Enzyme entrapment in reprecipitated polyaniline nano and microparticles. *Macromolecules* **43**, 4324–4330 (2010).
24. Lu, W., Elsenbaumer, R. L. & Wessling, B. Corrosion protection of mild steel by coatings containing polyaniline. *Synth. Met.* **71**, 2163–2166 (1995).
25. Lu, F., Wudl, F. & Nowak, M. Phenyl-capped octaaniline (COA): an excellent model for polyaniline. *J. Am. Chem. Soc.* **108**, 8311–8313 (1986).
26. Li, S., Dong, H. & Cao, Y. Synthesis and characterization of soluble polyaniline. *Synth. Met.* **29**, 329–336 (1989).
27. Huang, J., Virji, S. & Weiller, B. H. Polyaniline nanofibers: facile synthesis and chemical sensors. *J. Am. Chem. Soc.* **125**, 314–315 (2003).
28. Takashima, W., Kaneko, M., Kaneto, K. & MacDiarmid, A. G. The electrochemical actuator using electrochemically-deposited poly-aniline film. *Synth. Met.* **71**, 2265–2266 (1995).

29. Firmansyah, D. A. *et al.* Crystalline phase reduction of cuprous oxide (Cu_2O) nanoparticles accompanied by a morphology change during ethanol-assisted spray pyrolysis. *Langmuir* **25**(12), 7063–7071 (2009).
30. Risti, M., Ivanda, M. & Popovi, S. Dependence of nanocrystalline SnO_2 particle size on synthesis route. *J. Non Cryst. Solids* **303**, 270–280 (2002).
31. Mahesh, D. B., Raghumadhan, D., Basavaraj, S. & Venkataraman, A. Preparation and characterization of polyaniline–Co_3O_4 nanocomposites via interfacial polymerization. *Am. J. Mater. Sci.* **2**(3), 39–43 (2012).
32. Mahesh, D. B. *et al.* Preparation and characterization of Pani and Pani-Ag nanocomposites via interfacial polymerization. *Polym. Compd.* **30**, 1668–1677 (2009).
33. Ghodselahi, T., Vesaghi, M. A., Shafiekhani, A., Baghizadeh, A. & Lameii, M. XPS study of the Cu@Cu_2O core–shell nanoparticles. *Appl. Surf. Sci.* **255**, 2730–2734 (2008).
34. Huang, Z. *et al.* Continuous synthesis of size-tunable silver nanoparticles by green electrolysis method and multi-electrode design for high yield. *J. Mater. Chem. A* **3**, 1925–1929 (2015).
35. Boomi, P. & Prabu, H. G. Synthesis, characterization and antibacterial analysis of polyaniline/Au-Pd nanocomposite. *Colloids Surf. A Physicochem. Eng. Asp.* **429**, 51–59 (2013).
36. Blinova, N. V., Stejskal, J. & Trchova, M. The oxidation of aniline with silver nitrate to polyaniline–silver composites. *Polymer* **50**, 50–56 (2009).
37. Boomi, P., Gurumallesh, H. & Mathiyarasu, J. Synthesis and characterization of polyaniline/Ag–Pt nanocomposite for improved antibacterial activity. *Colloids Surf. B Biointerface* **103**, 9–14 (2013).
38. Tamboli, M. S. *et al.* Nanowires of silver–polyaniline nanocomposite synthesized via in situ polymerization and its novel functionality as an antibacterial agent. *Colloids Surf. B Biointerface* **92**, 35–41 (2012).
39. Ishaq, S. *et al.* Facile synthesis of ternary graphene nanocomposites with doped metal oxide and conductive polymers as electrode materials for high performance supercapacitors. *Sci. Rep.* **9**, 5974 (2019).
40. Feng, C., Chen, Z., Jing, J. & Hou, J. The photocatalytic phenol degradation mechanism of Ag-modified ZnO nanorods. J. Mater. Chem.C. (2020) Advance Article.
41. Jiang, H. Y. *et al.* Copper-based coordination polymer nanostructure for visible light photocatalysis. *Adv. Mater.* **28**(44), 9776–9781 (2016).
42. Zhao, G. *et al.* Polymer-based nanocomposites for heavy metal ions removal from aqueous solution: a review. *Polym. Chem.* **9**, 3562–3582 (2018).
43. Baghery, P., Farzam, M., Mousavi, A. B. & Hosseini, M. Ni–TiO_2 nanocomposite coating with high resistance to corrosion and wear. *Surf. Coat. Technol.* **204**, 3804–3810 (2010).
44. Raffi, M., Mehrwan, S. & Bhatti, T. M. Investigations into the antibacterial behavior of copper nanoparticles against *Escherichia coli*. *Ann. Microbiol.* **60**, 75–80 (2010).
45. Dibrov, P., Dzoiba, J., Gosink, K. K. & Häse, C. C. Chemiosmotic mechanism of antimicrobial activity of Ag(+) in Vibrio cholera. *Antimicrob. Agents Chemother.* **46**, 2668–2770 (2002).
46. Li, F., Lei, C. & Shen, Q. Analysis of copper nanoparticles toxicity based on a stress-responsive bacterial biosensor array. *Nanoscale.* **5**, 653–662 (2013).
47. Qasim, M., Udomluck, N. & Kim, K. Antimicrobial activity of silver nanoparticles encapsulated in poly-*N*-isopropylacrylamide-based polymeric nanoparticles. *Int. J. Nanomed.* **13**, 235–249 (2018).
48. Le, O. B. & Stellacci, F. Antibacterial activity of silver nanoparticles: a surface science insight. *Nano Today* **10**, 339–354 (2015).
49. Feng, Q. L., Wu, J. & Chen, G. Q. A mechanistic study of the antibacterial effect of silver ions on *Escherichia coli* and *Staphylococcus aureus*. *J. Biol. Mater. Res.* **52**, 662–668 (2000).

Acknowledgements

The author Sathish Mohan Botsa acknowledges the University Grants Commission (UGC) for Rajiv Gandhi National Fellowship (RGNF-SC-2016–17-AND-9309) to carry out this work as part of his Ph.D.

Author contributions

S.M.B., was responsible for conceptualisation, analysis, data interpretation and writing manuscript under the supervision of Co-author K.B.

Competing interests

The authors declare no competing interest.

Additional information

Supplementary information is available for this paper at https://doi.org/10.1038/s41598-020-70194-9.

Correspondence and requests for materials should be addressed to S.M.B. or K.B.

Reprints and permissions information is available at www.nature.com/reprints.

Publisher's note Springer Nature remains neutral with regard to jurisdictional claims in published maps and institutional affiliations.